JOURNAL OF AIRCRAFT
Vol. 37, No. 5, September–October 2000

Euler-Based Dynamic Aeroelastic Analysis of Shell Structures

Andrew P. Lewis*
University of Hertfordshire, Herts, England AL10 9AB, United Kingdom
and
Marilyn J. Smith†
Georgia Institute of Technology, Atlanta, Georgia 30332-0150

A computational aeroelastic method has been extended to evaluate the static and dynamic characteristics of flexible shell structures. The numerical method applied was the ENS3DAE solver, which permits evaluation of high-order aerodynamic and structure interactions. Modifications to the code to permit smooth transition of internal flowfield characteristics and deflections for shell structures have been developed and verified. The modified methodology has been tested on a problem of merit in the engine community, an axisymmetric engine liner that has exhibited dynamic instabilities. An investigation into the dynamic characteristics of the liner, including flutter, was carried out. The results were compared with experimental data and demonstrate the ability of the method to analyze shell flutter problems of this kind.

Introduction

FLEXIBLE structures must be modeled in computational methods if the dynamic response to loads is important. Because a structure undergoing aerodynamic loads does not remain rigid, computational solutions that assume rigid structures are providing inherently incorrect answers. When questions arise regarding fatigue, flutter, and other unsteady aeroelastic phenomena, the only recourse has been to employ aeroelastic methods with empirical or lower-order aerodynamic modules. Many times these computational alternatives are not accurate because the aerodynamic flowfield driving the phenomena is viscous- or vortex-dominated. Experimental studies provide the full flowfield physics, but they are very expensive, and there are difficulties in obtaining an understanding of the cause of the problem from the results. Thus, a computational method that combines higher-order aerodynamic predictive capabilities with flexible structures is desired.

These methods have been undergoing development and research applications for a number of years. Several proven methods exist and are used by government and industry to examine external aeroelastic problems, primarily lifting surface-based (wing-based) aeroelasticity.[1–3]

There exists another set of aeroelastic problems that appear to be driven by higher-order aerodynamics. These are propulsion-based problems where, instead of the classic plate representation for wing bending problems, a shell representation must be used. Experimental evidence indicates that shell instabilities in engine liners can be a problem.[4] This paper describes the extension of an external aeroelastic method ENS3DAE to handle the internal aerodynamics and shell structure for engine or propulsion problems. Results of the aeroelastic simulation correlated with experimental data are presented and discussed.

ENS3DAE Code Description

The ENS3DAE methodology was developed to examine a multitude of aeroelastic problems, primarily in the transonic flight regime. The solver was originally developed by the Lockheed–Georgia Company (now the Lockheed Martin Aeronautical Systems Group) for a variety of applications.[5–7] The solver was extended for aeroelastic applications by Lockheed in 1990 under contract to the U.S. Air Force[1,8] and has been undergoing extensions to examine different types of aeroelastic problems since that time.[9,10]

The aerodynamic module in ENS3DAE solves the full three-dimensional Reynolds-averaged Navier–Stokes equations for compressible flow, or simplifications of these equations, including the thin-shear-layer Navier–Stokes and the Euler equations. Both implicit time-accurate (fixed time step), or steady-state (spatially varying time step) options are employed via a time-marching fully implicit approximate factorization scheme. Boundary conditions are applied explicitly along the faces of each zone. O-, C-, and H-grid combinations can all be solved in this manner.

Aeroelastic analyses are obtained by coupling a set of structural dynamics equations of motion to the aerodynamic module. Pressures computed by the aerodynamic module act as forcing functions to the structural equations. The structural equations are solved using an explicit predictor–corrector scheme to compute the structural deflections. A shearing algorithm updates the aerodynamic grid using these calculated deflections. This procedure occurs at every aerodynamic time step, thus producing a tightly coupled, time-accurate aeroelastic solution. In addition the code conserves the geometric conservation law (GCL) when moving the grid. Although ENS3DAE can solve both structural influence coefficient and modal models, this paper is concerned only with the modal model. Further details of ENS3DAE can be obtained from Refs. 1 and 5–10.

The capability of the ENS3DAE program has been extended to include aeroelastic analysis of shell structures. Thus, the code can now be used to investigate engine liner flutter and divergence that has been known to occur and has been demonstrated experimentally.[4,11] The configuration considered here is shown in Fig. 1, which shows the nozzle of a jet engine. The engine liner is subject to airflow on both sides, where the flow in the annular region between the liner and the engine housing is cooler and of lower speed when compared with the inner core flow.

ENS3DAE Code Modifications

To analyze cylindrical shell problems, several modifications to the program were required. The flow outside and inside the engine liner structure was modeled by two blocks using cylindrical grids. The code was modified to update accurately a polar interface with a periodic boundary condition. Other aerodynamic module modifications included the improvement of inflow, outflow, and inviscid solid-surface boundary conditions, as well as a more exact flow initialization.

Received 1 January 1999; revision received 3 December 1999; accepted for publication 26 January 2000. Copyright © 2000 by Andrew P. Lewis and Marilyn J. Smith. Published by the American Institute of Aeronautics and Astronautics, Inc., with permission.

*Principal Lecturer, Department of Aerospace, Civil, and Mechanical Engineering.

†Assistant Professor, School of Aerospace Engineering. Associate Fellow AIAA.

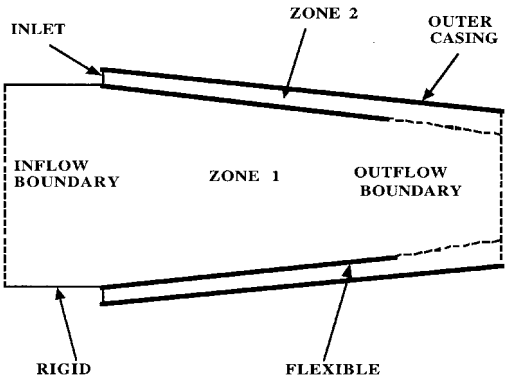

Fig. 1 Engine liner and exhaust nozzle.

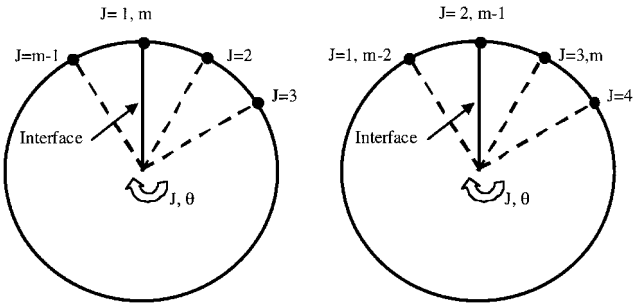

a) Original implementation **b) Modified implementation**

Fig. 2 Original and modified mesh points for a full cross section of the nozzle.

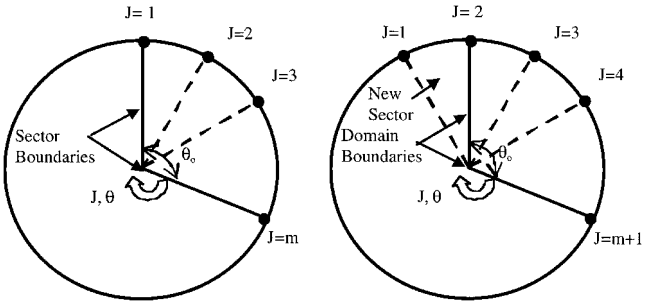

a) Original implementation **b) Modified implementation**

Fig. 3 Original and modified mesh points for an axisymmetric section of the nozzle.

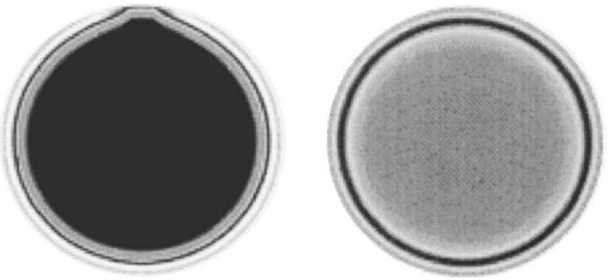

a) Original boundary condition **b) Modified boundary condition**

Fig. 4 Pressure distribution at a given cross section to check boundary condition smoothness.

Polar Interface Boundary Conditions

Boundary conditions in ENS3DAE are implemented explicitly. However, attempts to impose explicit polar boundary conditions for abutting grids were unsuccessful, and so a method for handling them using overlapping grids was devised. Two versions of these boundary conditions were implemented. The first assumed a full 360-deg mesh (necessary for asymmetric structural modes). The second enabled flow symmetries to be exploited by solving an arbitrary sector of the full flow domain, thus reducing the mesh size required for the problem. For these methods to work correctly, the user must specify a computational mesh having a one-cell overlap at the polar interface.

Consider a flow in an axisymmetric duct and let cylindrical coordinates (x, r, θ) be defined with the x axis lying along the centerline of the duct. When the physical domain is transformed into the computational domain, the axial, radial, and transverse coordinate directions (x, r, θ) will be taken to correspond to the I, K, and J directions, respectively, in computational space. A comparison of the two interfaces for explicit and implicit impositions of the boundary conditions is shown in Fig. 2. The original explicit, abutting grids are shown at a cross section of the duct in Fig. 2a. The polar interface boundary conditions were imposed across the end planes $J = 1$ and m that share a common interface. The boundary conditions were originally imposed by requiring that the flow variables have equal values on the planes $J = 1$ and m while the flow equations are solved across the interface.

To smoothly impose the polar interface boundary conditions implicitly, an overlapping sector was added, as shown in Fig. 2b. Now, the points $J = 1$ and 2 will be the same as points $J = m$ and $m + 1$, respectively. The flow variables at these pairs of points are now set equal so that $\boldsymbol{q}_1 = \boldsymbol{q}_m$ and $\boldsymbol{q}_{m+1} = \boldsymbol{q}_2$, where $\boldsymbol{q}$ is a column vector of the variables ρ, ρu, ρv, ρw, e. In addition, the flow equations are solved across the interface. For this, no modifications are required for sweeps of the algorithm in the I and K directions. However, in the J direction, the $m + 1$ by $m + 1$ block tridiagonal matrix that arises with explicit boundary conditions is modified so that if $A_{i,j}$ is the i, jth element of the matrix, then the elements $A_{2,m}$ and $A_{m,2}$ are now set equal to $A_{2,1}$ and $A_{m,m+1}$ respectively. Thus, a periodic block tridiagonal system is obtained.

Now consider a flow in an axisymmetric duct as before, but suppose that the flow is periodic in the sense that the flow conditions at (x, r, θ) are the same as those at $(x, r, \theta + \theta_0)$, where $n\theta_0 = 2\pi$ for some integer n. Then only the sector of the duct cross section subtended by θ_0 needs to be considered. Initially, the mesh at a cross section of the duct resembled Fig. 3a. The polar interface boundary condition was initially imposed explicitly across the end planes $J = 1$ and m, which were regarded as a common periodic interface. Thus, the boundary conditions required that the flow variables ρ, u, and e, together with the radial and transverse velocity components, have equal values on the planes $J = 1$ and m.

To smooth the flow across this interface, an extra sector was added to the mesh in the J direction as shown in Fig. 3b. Now the boundary conditions $q_1 = T\ q_m$ and $q_{m+1} = T^{-1}\ q_2$ are imposed explicitly, where T is a transformation matrix that resolves v and w in the radial and transverse directions. In addition, the flow equations are solved across the interface. Again, no modifications are required for sweeps of the algorithm in the I and K directions. However, in the J direction, the $m + 1$ by $m + 1$ block tridiagonal matrix that arises with explicit boundary conditions is modified in a manner similar to that for the case of a full duct cross section so that a periodic block tridiagonal system is obtained.

The resulting improvements from these modifications are seen for an axisymmetric case in Fig. 4. Figure 4a shows the original flow solution with the abutting formulation. Note that there is a numerically induced bump in the flow at the boundary condition. Figure 4b shows the result of the overlapping boundary conditions where there is no noticeable difference in the solution at any location in the duct cross section. This flow smoothness is particularly important in aeroelastic applications because pressure differences may induce nonphysical deflections in the liner.

Inflow/Outflow Riemann Invariant Boundary Conditions

Two sets of inflow and outflow boundary conditions were available in ENS3DAE, one set being specified in terms of the primitive variables u, v, w, ρ, and e, whereas the other is characteristics based. The primitive variable boundary conditions were found to give poor flow solution convergence characteristics, due to the reflection of waves from the outflow boundary, whereas the characteristics-based

boundary conditions were found to be far more satisfactory and so were used throughout this study. The boundary conditions were imposed in the standard implementation, using Reimann invariance. That is, having specified an initial flowfield, the physical inflow boundary conditions were defined by fixing the incoming Riemann invariant, whereas entropy and velocity components tangential to the inlet surface were set at values based on the local initial flowfield. Similar implementation of the boundary condition was made at the outflow condition. Details of the implementation can be found in any standard computational fluid dynamics (CFD) text.[12]

Euler Solid-Surface Boundary Condition

The Euler solid-surface boundary condition was replaced by a more robust set of conditions demonstrated by Donald Rizzetta at U.S. Air Force Research Laboratory (AFRL). In these boundary conditions, unit tangent vectors $\boldsymbol{t}_1$ and $\boldsymbol{t}_2$ and normal $\boldsymbol{n}$ to the surface at a point are first defined. At a point (i, j, k) on a solid boundary $k = \text{const}$, $\boldsymbol{t}_1$ is defined by normalizing the vector $\boldsymbol{x}_1$ connecting points $(i-1, j, k)$ and $(i+1, j, k)$. A further vector $\boldsymbol{x}_2$ is defined as that between points $(i, j-1, k)$ and $(i, j+1, k)$. Then $\boldsymbol{t}_1$, $\boldsymbol{n}$, and $\boldsymbol{t}_2$ are defined by

$$\boldsymbol{n} = \frac{\boldsymbol{x}_1 \times \boldsymbol{x}_2}{|\boldsymbol{x}_1 \times \boldsymbol{x}_2|}, \qquad \boldsymbol{t}_1 = \frac{\boldsymbol{x}_1}{|\boldsymbol{x}_1|}, \qquad \boldsymbol{t}_2 = \boldsymbol{n} \times \boldsymbol{t}_1 \tag{1}$$

The flow velocity at the point (i, j, ka), where ka gives the k surface adjacent to the solid boundary, is now resolved along the axis system defined by $\boldsymbol{t}_1$, $\boldsymbol{t}_2$, and $\boldsymbol{n}$. The slip velocity at the solid surface is then given by the velocity components along $\boldsymbol{t}_1$ and $\boldsymbol{t}_2$. This gave an implementation for rigid boundaries only, which was then modified for moving boundaries by adding a normal velocity component equal to the boundary grid velocity component along $\boldsymbol{n}$.

Flow Initialization

For internal flows, a typical flow initialization is based on quasi-one-dimensional flow theory. This was modified by taking the calculated flow velocity vector at each grid point (i, j, k) as lying along the vector connecting the grid points (i, j, k) and $(i+1, j, k)$. This gave an initial flowfield that came closer to satisfying the surface boundary conditions.

Engine Liner Application

A computational study was performed for the engine liner model investigated experimentally.[4] Note that, in addition to this particular study, there have been a number of other studies, both theoretical and experimental, of annular or internal flow-induced flutter and divergence of coaxial cylinders.[13–18] These have shown the type of aeroelastic instabilities that may be expected. However, the theoretical studies[13–17] consider only incompressible flow conditions and uniform cylinders, whereas aeroelastic instabilities for coaxial cylinders were investigated experimentally.[18] The capability developed here will enable far more general geometries and a wide range of flow regimes to be considered. The engine liner model is illustrated in Fig. 1. The liner's length is 56 mm; its radius is 45 mm at the fixed leading edge and 38.6 mm at its trailing edge. The distance between liner and outer casing is 1.82 mm, and the radius of the outer casing at the outlet is 37.2 mm. The liner is made of nickel and has a thickness of 0.1 mm. In this experiment, the liner was solid. In actual full-scale engines, the liners are perforated with holes, and, thus, a transpiration boundary condition would need to be applied to the liner. However, in this research, the goal was to reproduce numerically the experimental results, and so no transpiration was used.

The aeroelastic analysis was performed using mode shapes, generalized masses, and frequencies obtained from a NASTRAN finite element analysis. This analysis confirmed experimental structural vibration tests[4] showing that the lowest mode had a circumferential wave number $n = 6$; this is generally to be expected for shell structures that are relatively short.[19–21] Furthermore, the modes in the tests[4] experiencing the most excitation were those for $n = 6$–9. Accordingly, these modes were used in the subsequent aeroelastic analysis. Something not addressed in the present study was that the steady-state pressure loading and possibly viscous traction forces on the engine liner due to the flow can affect the structure's stiffness, which will in turn affect the aeroelastic predictions. In particular, increasing the inner flow Mach number will raise the stiffness, whereas increasing the outer annular flow Mach number will have a destiffening effect. However, the objective of the present study is to demonstrate the ability to predict flutter trends using Euler-based aerodynamic analysis, and for this the natural vibration modes of the liner were considered adequate. Another uncertainty that would make detailed comparisons difficult is the structural damping, which can affect shell flutter speeds significantly. Here, a critical damping ratio of 0.02 was applied to all modes. This ratio was the value measured experimentally.[4] Note that in this study structural nonlinearities, which become significant with increasing shell deflection amplitude, are not accounted for. However, here the conditions for onset of flutter prior to the impact of these structural nonlinearities were under study.

Results

Converged Rigid-Body Flow Solutions

Converged Euler solutions were obtained for a variety of flow conditions. These results were produced with a quarter flow domain model to take advantage of the rigid model's symmetry. The flow for the full domain was then expanded from the converged flow solution, and the program run again for a short number of iterations to confirm that the solution was correct.

Grid Sensitivity Study

A grid sensitivity study was first carried out for the case of steady-state flow. One quarter of the axisymmetric flow domain was modeled using two zones; one for the inner flow within the engine liner (zone 1) and one for the outer annular flow region (zone 2). Two grids were developed with sizes shown in Table 1, where $I_{\max}$, $J_{\max}$, and $K_{\max}$ are the number of nodes in the axial, circumferential, and radial directions, respectively. In both grids, clustering was imposed in the normal direction adjacent to the solid surfaces to ensure that the displacements and flow changes in the region would be adequately modeled. In the axial direction, the grid was uniformly distributed. In grid ii, the mesh around the engine liner trailing edge (both normal and streamwise), where the inner and outer flows first come into contact, was refined. Simulations for a flow having a Mach number at the liner trailing edge of 0.7 in the inner flow and 0.4 in the annular region were used for the comparison. A comparison of the results is presented in terms of nondimensional pressure distribution along the inner and outer surfaces of the engine liner in Figs. 5 and 6. Pressure here is nondimensionalized by reference values of density and speed of sound.

Figures 5 and 6 show good agreement between pressure distributions obtained with the two grids. Lift, drag, and pitching moment coefficients were also calculated for the two grids, referenced by the surface area and length of the quarter of the engine liner modeled. A comparison of the results is shown in Table 2. Agreement may be

Table 1 Number of nodes per zone per grid

Grid–zone	$I_{\max}$	$J_{\max}$	$K_{\max}$
i–1	73	26	33
i–2	64	26	23
ii–1	93	26	45
ii–2	79	26	30

Table 2 Comparison of force and moment coefficients determined using grids i and ii

Coefficient	Grid i	Grid ii	Percentage difference
C_L	−0.1096	−0.1132	3.2
C_D	0.0138	0.0143	3.5
C_m	0.0707	0.0729	3.0

Table 3 Inner and annular region flow Mach numbers

Case	M_i	M_o	q_o, bar
a	0.7	0.4	0.13
b	0.7	0.7	0.34
c	0.4	0.1	0.01
d	0.4	0.4	0.13
e	0.4	0.7	0.34

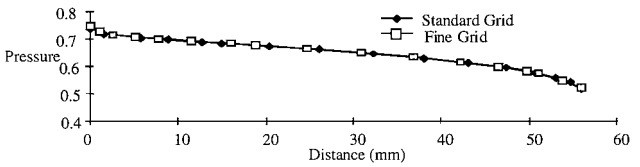

Fig. 5 Pressure distribution on liner outer surface.

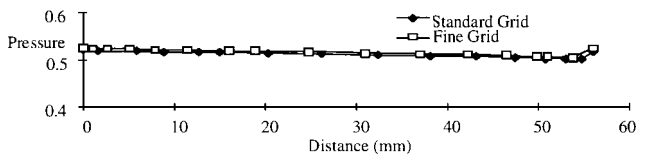

Fig. 6 Pressure distribution on liner inner surface.

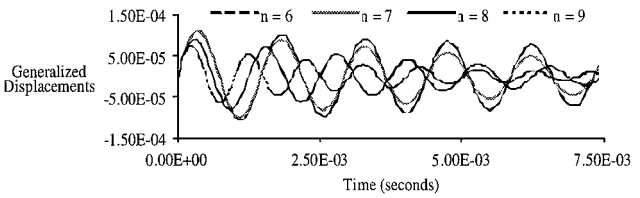

Fig. 7 Engine liner modal aeroelastic response for case a.

seen to be close, therefore the aeroelastic study was accomplished using grid i.

Aeroelastic Analysis

This section presents results from aeroelastic analysis of the engine liner configuration. The dynamic response of the structure was investigated using the natural modes with circumferential wave numbers $n = 6$–9 as described earlier. Results for five flow conditions are presented and compared with the experimental results.[4] These results show the point of flutter onset for different inner flow Mach numbers M_i at the engine liner trailing edge as the dynamic pressure of the outer annular region flow at the engine liner trailing edge is increased. Five cases are considered as shown in Table 3, where M_o is the flow Mach number in the annular region at the engine liner trailing edge and q_o is the corresponding dynamic pressure.

A full domain model was used because the circumferential wave numbers of the modes used indicate that no symmetries are present. A Courant–Friedrichs–Lewy (CFL) of 5.0 was used for both rigid and dynamic simulations. For each case, the first step was to obtain a converged steady-state flow solution. Aeroelastic responses were obtained by specifying an initial velocity disturbance for each generalized velocity. As an example of the kind of response obtained, results for case a are given in Fig. 7 in terms of time histories of the four generalized coordinates. The results show the engine liner to be dynamically stable. The corresponding radial displacement of a typical point on the trailing edge of the engine liner is shown in Fig. 8. The peak displacements of the structure are of the same order of magnitude as its thickness. The form of the response, given that all modes have been excited by the initial conditions used, is due to phase shifts between the superposed modes. Similar runs were carried out for cases b, c, d, and e, and the responses in each mode were then studied. Comparisons of the effect of varying the outer flow conditions while keeping the inner flow the same were first

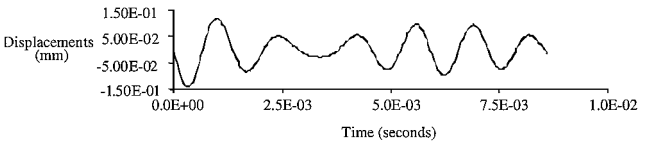

Fig. 8 Radial displacement of a point on the engine liner trailing edge for case a.

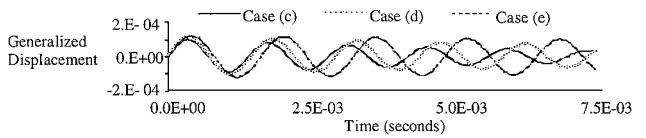

Fig. 9 Comparison of aeroelastic responses in mode $n = 6$ for varying outer flow conditions.

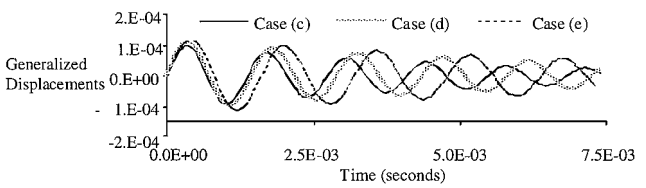

Fig. 10 Comparison of aeroelastic responses in mode $n = 7$ for varying outer flow conditions.

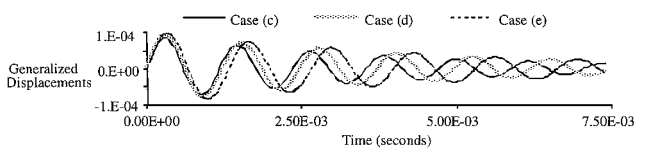

Fig. 11 Comparison of aeroelastic response in mode $n = 8$ for varying outer flow conditions.

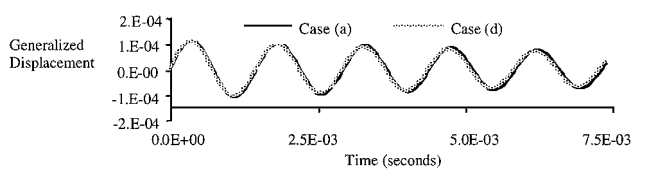

Fig. 12 Comparison of aeroelastic responses in mode $n = 6$ for varying inner flow speeds.

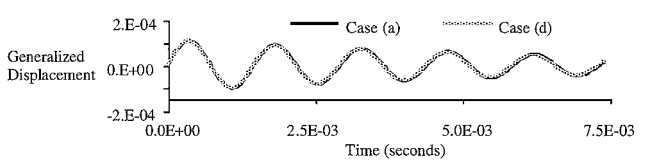

Fig. 13 Comparison of aeroelastic responses in mode $n = 7$ for varying inner flow speeds.

made. These are shown in Figs. 9–11, where cases c, d, and e are compared. These show that the outer flow conditions significantly affect the aeroelastic behavior. A comparison for the lowest mode ($n = 6$) for the three cases is shown in Fig. 9. Figure 9 indicates that case e is only just dynamically stable. Cases c and d are more dynamically stable than case e, and this behavior is consistent with the experimental results.[4] Figures 10 and 11 compare the aeroelastic responses in the three cases for modes $n = 7$ and 8. In all cases, the response is dynamically stable and the effect of increasing M_o appears less significant than for $n = 6$. Case c considers a very low outer flow Mach number and shows that the effect of this is to make the response more heavily damped than in the other cases.

Comparisons of the effect of varying the inner flow conditions while keeping the outer flow fixed were now made. Results for cases a and d, where the outer flow Mach number is 0.4, are shown in terms of the modal responses for circumferential wave numbers $n = 6$–8 in Figs. 12–14. Figures 12–14 show that the responses are almost identical, indicating that the inner flow Mach number over the range

Table 4 Comparison of experimental and predicted engine liner natural frequencies

Wave number n	Natural frequencies, Hz	
	Test	NASTRAN
6	687.0	755.5
7	763.0	763.3
8	904.0	878.0
9	1080.0	1061.0

Table 5 Frequencies of engine liner responses

Wave number n	Case a, 4 modes	Case b, 4 modes	Case b, 1 mode	Case c, 4 modes	Case d, 4 modes	Case e, 4 modes
6	683.3	639.5	641.9	723.7	686.0	622.3
7	683.3	636.0	——	733.0	686.0	626.9
8	801.5	759.9	——	853.0	803.6	751.8
9	994.4	956.4	——	1040.7	991.3	956.9

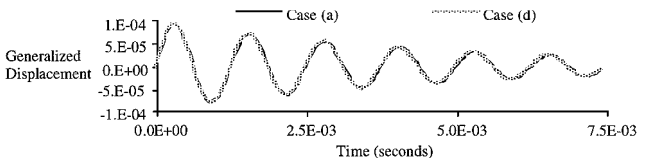

Fig. 14 Comparison of aeroelastic responses in mode $n = 8$ for varying inner flow speeds.

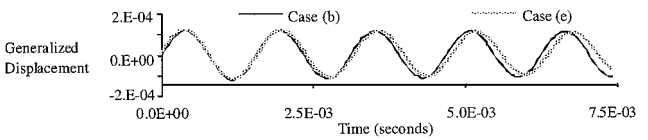

Fig. 15 Comparison of aeroelastic responses in mode $n = 6$ for varying inner flow conditions; $M_o = 0.7$.

of conditions considered has little effect on the aeroelastic response. Because static pressure loading effects on the liner stiffness are not accounted for in this study, these may lead to larger differences in the responses than those predicted here.

A further study of the effect of varying inner flow conditions was conducted for the situation where the aeroelastic response is only just dynamically stable. Thus, the outer flow Mach number was taken as 0.7, where, for case e, the engine liner response is close to neutral stability. A comparison of the response in mode $n = 6$ for cases b and e is shown in Fig. 15. This shows that increasing the inner flow Mach number is slightly destabilizing, but, again, confirms that the engine liner aeroelastic response is more sensitive to changes in the outer flow conditions. The aeroelastic response in case b ties in with the experimental results.[4] Given that the inner flow condition is $M_i = 0.7$, whereas for the outer flow $q_o \approx 0.34$ bar, this result fits in well with the experimental results.[4] These showed that for $M_i = 0.6$, flutter onset occurs when $q_o \approx 0.25$ bar, whereas when $M_i = 0.85$, flutter onset occurs when $q_o \approx 0.39$ bar.

The natural frequencies of the engine liner structure, as measured in the tests[4] and as predicted by theory, are shown in Table 4. These are seen to agree well. The frequencies and damping of the modal responses for the five cases are summarized in Tables 5 and 6. The calculated frequencies for modes $n = 6$ and 7 are very close together and in the aeroelastic responses for cases a and d become almost identical. As M_o increases, the frequencies drop, in agreement with the experiment. It is anticipated that for a sufficiently high dynamic pressure q_o, divergence in the mode $n = 6$ will eventually occur. Because the effects of steady pressure loading on the stiffness of the liner have not been included, a precise estimate of divergence dynamic pressure cannot be made. These numerical results tend

Table 6 Modal damping of engine liner response

Wave number n	Case a, 4 modes	Case b, 4 modes	Case b, 1 mode	Case c, 4 modes	Case d, 4 modes	Case e, 4 modes
6	0.015	0.003	0.003	0.032	0.017	0.007
7	0.031	0.025	——	0.042	0.032	0.029
8	0.043	0.041	——	0.047	0.042	0.042
9	0.048	0.048	——	0.049	0.047	0.048

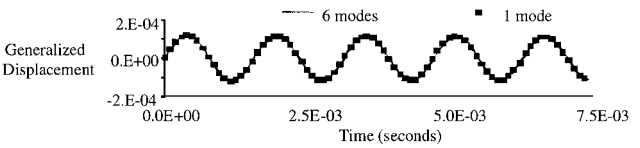

Fig. 16 Effect of number of modes on aeroelastic responses for case b; $M_i = 0.7$ and $M_o = 0.7$.

to confirm the experimental conclusions[4] that instabilities in the flowfield are initiated by one mode in the outer flow.

The results also make clear the sensitivity of the flutter boundary to structural damping. Cases a, b, d, and e would be dynamically unstable in the absence of the engine liner structural damping, and only case c would still be stable. This feature of shell flutter problems involving annular flow was highlighted both in the engine liner tests[4] and in one of the aforementioned theoretical studies involving coaxial cylinders.[17]

The closeness of the frequencies of the modes $n = 6$ and 7 suggests the possibility that the cause of the flutter predicted here is due to the interaction of two coupled modes rather than a single-degree-of-freedom flutter. To investigate whether any modal interaction was occurring, a run for one set flow conditions was repeated. Case b was reevaluated using only mode $n = 6$ because earlier observations noted that this mode yielded deflections close to dynamic instability. A comparison between the engine liner response for mode 6 alone and for all modes present is presented in Fig. 16. The responses shown are very similar. It is apparent from Tables 5 and 6 that the modal frequency is altered only slightly and, more importantly, that the damping is almost unaffected by the presence of the higher modes. It is concluded from this result that single-mode flutter is occurring. This suggests the possibility of conducting future studies with a reduced model representing one circumferential wavelength of the critical mode only. This would result in significant runtime savings in future studies by taking advantages of symmetry.

Conclusions

The Euler/Navier–Stokes solver ENS3DAE has been extended to enable the aeroelastic behavior of shell structures to be analyzed. The code has been applied in an investigation of engine liner flutter using a test configuration for which experimental results are available. This is the first time that an aeroelastic solver using higher-order aerodynamics has been applied to flexible shells, in particular this engine liner problem. The results obtained are promising and demonstrate the ability of this and similar methods to analyze shell flutter problems. To enable more detailed comparisons to be made, the effects of steady pressure loads on shell structure stiffness need to be taken into account. This could be achieved by using pressure loading from steady-state runs in the external structural analysis to determine the frequencies and mode shapes. Thus, no additional modifications to ENS3DAE would be required. The impact of viscous effects also would not require additional modifications to the code.

Acknowledgments

Thanks are due to the University of Hertfordshire who supported Andrew P. Lewis's secondment to the Georgia Institute of Technology during 1997. This work was partially funded by the U.S. Air Force Research Laboratory (AFRL) under Contract F33615-90-C-3211. The technical monitor, Larry Huttsell, was especially helpful by providing the NASTRAN inputs and for his insightful comments. Thanks are also due to Phil Beran and Donald Rizzetta of AFRL, who suggested the improved Euler boundary conditions.

References

[1]Schuster, D. M., Vadyak, J., and Atta, E., "Flight Loads Prediction Methods for Fighter Aircraft," Wright Research and Development Center, WRDC-TR-89-3104, Dayton, OH, Nov. 1989.

[2]Rickets, R. H., Noll, T. E., Whitlow, W., and Huttsell, L. J., "Overview of Aeroelasticity Studies for the National Aero-Space Plane," AIAA Paper 93-1313, April 1993.

[3]Byun, C., and Guruswamy, G. P., "A Comparative Study of Serial and Parallel Aeroelastic Computations of Wings," NASA TM 108805, Jan. 1994.

[4]Ziada, S., Buhlmann, E. T., and Bolleter, U., "Model Tests on Shell Flutter Due to Flow on Both Sides," *Journal of Fluids and Structures*, Vol. 2, 1988, pp. 177–196.

[5]Vadyak, J., and Smith, M. J., "Simulation of Engine Installation Flowfields Using a Three-Dimensional Euler/Navier–Stokes Algorithm," AIAA Paper 86-1537, June 1986.

[6]Vadyak, J., Smith, M. J., Schuster, D. M., and Weed, R., "Simulation of External Flowfields Using a Three-Dimensional Euler/Navier–Stokes Algorithm," AIAA Paper 87-0484, Jan. 1987.

[7]Vadyak, J., Smith, M., Schuster, D., and Shrewsbury, G., "Simulation of Aircraft Component Flowfields Using a Three-Dimensional Navier–Stokes Algorithm," Third International Symposium on Science and Engineering on Cray Supercomputers, Cray Research, Inc., Minneapolis, MN, Sept. 1987.

[8]Schuster, D. M., Vadyak, J., and Atta, E., "Static Aeroelastic Analysis of Fighter Aircraft Using a Three-Dimensional Navier–Stokes Algorithm," *Journal of Aircraft*, Vol. 27, No. 9, 1990, pp. 820–825.

[9]Schuster, D. M., "Application of a Navier–Stokes Aeroelastic Method to Improve Fighter Wing Performance at Maneuver Flight Conditions," AIAA Paper 93-0529, Jan. 1993.

[10]Smith, M. J., Schuster, D. M., Huttsell, L., and Buxton, B., "Development of an Euler/Navier–Stokes Aeroelastic Method for Three-Dimensional Vehicles with Multiple Flexible Surfaces," AIAA Paper 96-1400, April 1996.

[11]Ahuja, K. K., Manes, J., and Massey, K., "Supersonic Jet Noise Reduction from Single and Coaxial Rectangular Jets," Final Rept. NASA Grant NAG3-1066, NASA John H. Glenn Research Center at Lewis Field, Cleveland, OH, Feb. 1992.

[12]Anderson, D. A., Tannehill, J. C., and Pletcher, R. H., *Computational Fluid Mechanics and Heat Transfer*, McGraw–Hill, New York, 1984, pp. 259–272.

[13]Paidoussis, M. P., Misra, A. K., and Chan, S. P., "Dynamics and Stability of Coaxial Cylindrical Shells Conveying Viscous Fluid," *Journal of Applied Mechanics*, Vol. 52, No. 2, 1985, pp. 389–396.

[14]El Chebair, A., Misra, A. K., and Paidoussis, M. P., "Theoretical Study of the Effect of Unsteady Viscous Forces on Inner- and Annular-Flow-Induced Instabilities of Cylindrical Shells," *Journal of Sound and Vibration*, Vol. 138, No. 3, 1990, pp. 457–478.

[15]Paidoussis, M. P., Misra, A. K., and Nguyen, V. B.,"Internal- and Annular-Flow-Induced Instabilities of a Clamped–Clamped or Cantilevered Cylindrical Shell in a Coaxial Conduit: The Effects of System Parameters," *Journal of Sound and Vibration*, Vol. 159, No. 2, 1992, pp. 193–205.

[16]Nguyen, V. B., Paidoussis, M. P., and Misra, A. K., "A CFD-Based Model for the Study of the Stability of Cantilevered Coaxial Cylindrical Shells Conveying Viscous Fluid," *Journal of Sound and Vibration*, Vol. 176, No. 1, 1994, pp. 105–125.

[17]Paidoussis, M. P., Nguyen, V. B., and Misra, A. K., "A Theoretical Study of the Stability of Cantilevered Coaxial Cylindrical Shells Conveying Fluid," *Journal of Fluids and Structures*, Vol. 5, 1991, pp. 127–164.

[18]Nguyen, V. B., Paidoussis, M. P., and Misra, A. K., "An Experimental Study of the Stability of Cantilevered Coaxial Cylindrical Shells Conveying Fluid" *Journal of Fluids and Structures*, Vol. 7, No. 8, 1993, pp. 913–930.

[19]Leissa, A. W., "Vibration of Shells," NASA SP-288, 1975.

[20]Irie, Y., Yamada, G., and Kaneko, Y., "Free Vibration of a Conical Shell with Variable Thickness," *Journal of Sound and Vibration*, Vol. 72, No. 1, 1982, pp. 83–94.

[21]Soedel, W., "A New Frequency Formula for Closed Circular Cylindrical Shells for a Large Variety of Boundary Conditions," *Journal of Sound and Vibration*, Vol. 70, No. 3, 1980, pp. 309–317.